Niiranen, Jarkko; Balobanov, Viacheslav; Kiendl, Josef; Hosseini, S. B.

Variational formulations, model comparisons and numerical methods for Euler–Bernoulli micro- and nano-beam models

Published in:
MATHEMATICS AND MECHANICS OF SOLIDS

DOI:
10.1177/1081286517739669

Published: 01/01/2019

Document Version
Peer reviewed version

Please cite the original version:
Niiranen, J., Balobanov, V., Kiendl, J., & Hosseini, S. B. (2019). Variational formulations, model comparisons and numerical methods for Euler–Bernoulli micro- and nano-beam models. *MATHEMATICS AND MECHANICS OF SOLIDS*, *24*(1), 312-335. https://doi.org/10.1177/1081286517739669

Journal Title
XX(X):2–33

DOI: 10.1177/ToBeAssigned
www.sagepub.com/

Variational formulations, model comparisons and numerical methods for Euler–Bernoulli micro- and nano-beam models

J. Niiranen[1], V. Balobanov[1], J. Kiendl[2] and S. B. Hosseini[1]

Abstract

As the first step, variational formulations and governing equations with boundary conditions are derived for a pair of Euler–Bernoulli beam bending models following a simplified version of Mindlin's strain gradient elasticity theory of form II. For both models, this leads to sixth-order boundary value problems with new types of boundary conditions which are given additional attributes *singly* and *doubly*; referring to a physically relevant distinguishment between free and prescribed curvature, respectively. Second, the variational formulations are analyzed with rigorous mathematical tools: existence and uniqueness of weak solutions are established by proving continuity and ellipticity of the associated symmetric bilinear forms. This guarantees optimal convergence for conforming Galerkin discretization methods. Third, the variational analysis is extended to cover two other generalized beam models: another modification of the strain gradient elasticity theory and a modified version of the couple stress theory. A model comparison reveals essential differences and similarities in the physicality of these four closely related beam models: they demonstrate essentially two different kinds of parameter-dependent stiffening behavior – one of these kinds (possessed by three models out of four) provides results in a very good agreement with size effects of experimental tests. Finally, numerical results for isogeometric Galerkin discretizations with B-splines confirm the theoretical stability and convergence results. Influences of the gradient and thickness parameters connected to size effects, boundary layers and dispersion relations are studied thoroughly with a series of benchmark problems for statics and free vibrations. Size-dependency of the effective Young's modulus is demonstrated for an auxetic cellular metamaterial ruled by bending-dominated deformation of cell struts.

Keywords
Strain gradient elasticity, couple stress theory, size effects, Euler–Bernoulli beams, Galerkin formulations, convergence analysis, auxetics

1. Introduction

Micro- and nano-sized beams, plates and membranes are the key structural components in sensors and actuators of micro-electromechanical systems (MEMS) and nano-electromechanical systems (NEMS) of today and the future [1–6]. In particular, developments in micro-machining and additive manufacturing at meso-, micro- and nano-scales intrinsically increase the potential of printed small-scale electro-mechanical devices [7]. A specific application field in which micro- and nano-sized beams have a crucial role is auxetic cellular metamaterials with numerous cell topologies formed by straight or curved struts [8,9]. These metamaterials share a common fundamental feature: auxeticity is governed by bending-dominated deformation of cell struts. From the point of view of engineering analysis – material science and applied mechanics, primarily – one of the key challenges in analyzing micro- and nano-sized structures is that the microstructural lengths of the material such as crystal size become comparable to the dimensions of the structure itself such as the beam thickness. In general, this means the necessity of multi-scale mechanics and implies a need for reliable and efficient multi-scale analysis tools, both analytical and computational methods alongside with experimental tests [4,5,10–12].

Classical continuum mechanics, as a well-established field with reliable and efficient computational tools, have been applied for modeling even nano-scale structures in different ways [13], besides computationally costly atomistic simulations [4,5,10]. Most typically, atomistic lattices are simply replaced by grids of classical springs, rods or struts with point masses. Or homogenization techniques are used by adopting classical plate or shell models [10,11,14] – even as straightforwardly as by applying commercial finite element software tools [15]. However, the classical continuum theory behind the classical dimensionally reduced structural models is actually not capable of describing multi-scale phenomena due to the underlying well-defined axioms of the homogenizing conception of Cauchy's continuum. Accordingly, the classical continuum theories have been extended towards multi-scale capabilities in different ways (see [16,17] and [18–22] for introductory reviews and further references).

Regarding micro- and nano-sized beams which are of our particular interest [23], it has been experimentally shown that especially the normalized elastic bending rigidity dramatically increases alongside decreasing thickness. In the elastic range, this

[1] Aalto University, Department of Civil Engineering, Espoo, Finland
[2] Norwegian University of Science and Technology, Department of Marine Technology, Trondheim, Norway

Corresponding author:
Jarkko Niiranen, Aalto University, Department of Civil Engineering, P.O. Box 12100, 00076 AALTO, Finland
Email: jarkko.niiranen@aalto.fi

microstructural size effect has been observed for micro-sized cantilever beams[24–26] and nano-sized clamped beams[27]: for epoxy catilever beams[24]; for polypropylene cantilevers[25]; and very recently for epoxy and epoxy-based SU-8 cantilevers[26]. Silver and ZnO nanowires have been studied in[27] and[28], respectively. Another type of MEMS-related validation can be found in[29].

Alongside the observations on the experimental bending tests of micro-cantilevers, a number of closely related theoretical works on generalized Euler–Bernoulli beam bending models exist in the literature: first, Papargyri–Beskou et al.[30] (2003) introduced a model based on a simplified one-parameter strain gradient theory originally proposed by Vardouolakis et al.[31] and Altan and Aifantis[32] with a one-parameter surface energy extension[31,33]; second, Park and Gao[34] (2006) proposed a one-parameter model by following a modified couple stress theory[35], later extended by Gao and Mahmoud[36] (2014) by a surface energy part originating from[37]; third, the three-parameter model proposed by Kong et al.[38] (2009) and Akgös and Civalek[39] (2012) is based on a modified strain gradient elasticity theory[24] (following Mindlin's strain gradient elasticity theory of form I); fourth, the one-parameter model derived by Lazopoulos and Lazopoulos[40] (2010) and Liang et al.[41] (2014) is based on the simplified strain gradient elasticity theory of[31–33,42]. Some of these models have been extended to shear-deformable Timoshenko beams or other higher-order variants, even including anisotropy (see[43–46], for instance). On the other hand, it should be noticed that scale-independent but microstructure-dependent behavior of beam-like structures have been studied via homogenization procedures resulting in different non-standard higher-gradient models, with size-dependent effective stiffness parameters, in particular[47–50]. Altogether, a preference seems to clearly be given to simple models of few additional parameters for two reasons: models should be validable; benchmark problems should be solvable by analytical means. The four generalized models listed above will be revisited and further analyzed in the present contribution. Our primary focus is on the pair of beam models (the first and fourth in the listing above) based on the widely-used simplified theory of strain gradient elasticity which (without surface energy terms) can be regarded as a single-parameter version of the Mindlin's strain gradient elasticity theory of form II derived in the landmark paper[51] in the 1960s. From the mathematical point of view, the models listed above, except the couple stress one, lead to sixth-order differential equations in contrast to the fourth-order equation of the classical Euler–Bernoulli beam model. The mathematical similarity of the models serves as our motivation for the first part of this work proposing variational formulations and analysis as well as addressing the differences and similarities in the physicalities of these models.

So far, solely analytical solutions for a limited number of simple benchmark problems have been presented in the literature concerning generalized beam bending models, as recently noticed in[52] proposing a semi-analytical displacement method. Numerical methods providing tools for solving complex problems are practically missing as concluded in a very recent review on generalized beam and plate models[53]:"*...most of existing size-dependent models focused on analytical solutions...limited to beam and plate structures subjected to certain loading and boundary conditions and geometries...*

Therefore, further efforts should be devoted to developing finite element models of size-dependent theories, especially the strain gradient-based models." Most likely, the lack of contributions proposing numerical methods for gradient-based models stems from the fact that the traditional finite element methods with polynomial basis functions, such as the C^0-continuous Lagrange or C^1-continuous Hermite ones, are not appropriate for higher-order problems. This serves as our motivation for the second part of this work providing a theoretical framework for reliable and efficient general-purpose numerical methods, including a proposal of such a method with a rigorous numerical analysis of the method, a verification of the implementation, and finally a series of benchmark problems for statics and free vibrations. In particular, the benchmarks demonstrate the influences of the gradient and thickness parameters connected to size effects, boundary layers and dispersion relations.

It should be mentioned that for micro- and nano-structures such as nanotubes and graphene sheets, in particular, the so-called non-local continuum theory has raised attention among reseachers of the field as well (see [12,20] for selective but still extensive lists of references and [53] for a more comprehensive review). However, a concern about the non-local continuum theory – discovered particularly in the context of non-local beam models – is the fact that a big portion of the literature applies the so-called differential form of Eringen's constitutive equation [54] which is very recently shown to be nonequivalent to its integral form in the context of Euler–Bernoulli beam problem [20] (see [55] as well). As a matter of fact, this nonequivalence is shown to be the reason for the discrepancy between the results of beam bending problems with different boundary conditions (see the discussion about the "paradox" in [20] and the references therein).

In this work, by following the simplified strain gradient elasticity theory we first use the principle of virtual work and derive two variants (cf. [40,41] and [30]) of governing equations and complete sets of essential and natural boundary conditions distinguishing fixings *singly* and *doubly*; referring to a physically meaningful separation between free and prescribed curvature, respectively. An analogous separation has been accomplished by Niiranen and Niemi for Kirchhoff plates [18] and Niiranen et al. [56] for bars and plane strain/stress problems. Second, we propose the corresponding displacement form variational formulations and prove their well-posedness with rigorous mathematical tools within an H^3 Sobolev space setting. For conforming Galerkin discretization methods, in particular, this guarantees invertible stiffness matrices and optimal convergence. Third, we accomplish a model comparison between the four model variants and show that our variational analysis can be extended to the other two generalized beam models as well ([34] and [38,39]). Furthermore, the analysis can be even extended to the single-variable locking-free formulation introduced for classical Timoshenko beams in [57]. The model comparison reveals that the generalized beam models demonstrate two different kinds of parameter-dependent stiffening behavior – one of these kinds (possessed by three models out of four) enables a very good agreement with experimental results. Finally, we adopt isogeometric B-spline basis functions of order $p \geq 3$ for implementing a C^{p-1}-continuous, H^3-conforming numerical method. An analogous approach has been very recently adopted for gradient-elastic Kirchhoff plates by Niiranen et al. [58]. With numerical benchmarks, we confirm our theoretical convergence results and illustrate the

most essential features of the beam models. For applying isogeometric analysis (IGA) to higher-order partial differential equations of structural dimension reduction models, within both classical and generalized continua, we refer to[56,58–62] (including introductory reviews on IGA). As a special application, size dependency of the effective Young's modulus is demonstrated for an auxetic cellular metamaterial relying on bending-dominated deformation of cell struts. For this example, modified couple stress model and finite elements with C^1-continuous Hermite basis functions are applied.

This paper is organized as follows: In Section 2, we recall the theory of strain gradient elasticity applied to the Euler–Bernoulli beam bending model. In Section 3, we derive the strong forms of the problem, whereas Section 4 is devoted to variational formulations, stability analysis, numerical methods and error analysis. Section 5 is devoted to model comparisons. In Section 6, we set up an isogeometric Galerkin discretization for numerical benchmarks and examples. Conclusions are finally drawn in Section 7.

2. Continuum models

This section recalls the strain gradient theory of a linearly isotropic elastic continuum and its application to the Euler–Bernoulli beam bending model.

Strain gradient elasticity theory

Let us first consider Mindlin's strain gradient elasticity theory of form II[51] giving the strain energy density in the form (equation (11.3) in[51])

$$\begin{aligned}\mathcal{W}_{II} = \frac{1}{2}\lambda\varepsilon_{ii}\varepsilon_{jj} + \mu\varepsilon_{ij}\varepsilon_{ij} + g_1\gamma_{iik}\gamma_{kjj} + g_2\gamma_{ijj}\gamma_{ikk} \\ + g_3\gamma_{iik}\gamma_{jjk} + g_4\gamma_{ijk}\gamma_{ijk} + g_5\gamma_{ijk}\gamma_{kji},\end{aligned} \tag{1}$$

where the (third-order) micro-deformation tensor is defined as the strain gradient

$$\boldsymbol{\gamma} = \boldsymbol{\nabla}\boldsymbol{\varepsilon}, \tag{2}$$

where operator $\boldsymbol{\nabla}$ denotes the third-order tensor-valued gradient and the classical linear strain tensor is defined as

$$\boldsymbol{\varepsilon} = \boldsymbol{\varepsilon}(\boldsymbol{u}) = \frac{1}{2}\big(\boldsymbol{\nabla}\boldsymbol{u} + (\boldsymbol{\nabla}\boldsymbol{u})^T\big), \tag{3}$$

with the nabla operator denoting now the second-order tensor-valued gradient. The work conjugate quantity of the micro-deformation, the (third-order) double stress tensor, is defined by a set of five non-classical material parameters $g_1 = g_1(x,y,z), ..., g_5 = g_5(x,y,z)$ ($\hat{a}_i$ in Mindlin's notation) as $\tau_{ijk} = \partial\mathcal{W}_{II}/\partial\gamma_{ijk} = \tau_{jik}$ with indices $i,j,k = x,y,z$ for Cartesian coordinates x,y,z. The classical Cauchy stress tensor $\boldsymbol{\sigma}$, in turn, is related to its work conjugate as $\sigma_{ij} = \partial\mathcal{W}_{II}/\partial\varepsilon_{ij}$ through the generalized Hooke's law

$$\boldsymbol{\sigma} = 2\mu\boldsymbol{\varepsilon} + \lambda\mathrm{tr}\,\boldsymbol{\varepsilon}\boldsymbol{I}, \tag{4}$$

with Lamé material parameters $\mu = \mu(x, y, z)$ and $\lambda = \lambda(x, y, z)$ and $\boldsymbol{I}$ denoting the identity tensor. The displacement field of body $\mathcal{B}$ is denoted by $\boldsymbol{u} : \mathcal{B} \to \mathbb{R}^3$. Consequently, the virtual work expression is written in the form (cf. equation (11.7) in[51])

$$\delta W_{\text{int}} = \int_{\mathcal{B}} \boldsymbol{\sigma} : \boldsymbol{\varepsilon}(\delta \boldsymbol{u}) \, \mathrm{d}\mathcal{B} + \int_{\mathcal{B}} \boldsymbol{\tau} \vdots \boldsymbol{\gamma}(\delta \boldsymbol{u}) \, \mathrm{d}\mathcal{B}, \tag{5}$$

where : and $\vdots$ denote the scalar products for second- and third-order tensors, respectively. Applying the Einstein summation convention, these products are defined as $\boldsymbol{\sigma} : \boldsymbol{\varepsilon} = \sigma_{ij}\epsilon_{ij}$ $\boldsymbol{\tau} \vdots \boldsymbol{\gamma} = \tau_{ijk}\gamma_{ijk}$.

A one-parameter simplified strain gradient elasticity theory proposed originally by Altan and Aifantis[32] considers from (1) only the non-classical terms which are related to parameters g_3 and g_4 by reducing the strain energy density (1) to (equation (5) in[32])

$$\mathcal{W}_{II} = \frac{1}{2}\lambda\varepsilon_{ii}\varepsilon_{jj} + \mu\varepsilon_{ij}\varepsilon_{ij} + g^2\big(\frac{1}{2}\lambda\varepsilon_{ii,k}\varepsilon_{jj,k} + \mu\varepsilon_{ij,k}\varepsilon_{ij,k}\big), \tag{6}$$

where the non-classical material parameter g describes the length scale of the micro-structure of the material. Double-stresses

$$\tau_{ijk} = \frac{\partial \mathcal{W}_{II}}{\partial \varepsilon_{ij,k}} = g^2(\lambda\varepsilon_{ll,k}\delta_{ij} + 2\mu\varepsilon_{ij,k}) = \tau_{jik} \tag{7}$$

are related to strain derivatives by the Lamé parameters and the gradient parameter g ($g_3 = g^2\lambda/2, g_4 = g^2\mu$). For constant Lamé parameters, (7) gives the double stress tensor in the form $\boldsymbol{\tau} = g^2\boldsymbol{\nabla}\boldsymbol{\sigma}$, (cf.[42] and the energy postulate in[63]) and finally with (2) the virtual work expression (5) in the form

$$\delta W^g_{\text{int}} = \int_{\mathcal{B}} \boldsymbol{\sigma} : \boldsymbol{\varepsilon}(\delta \boldsymbol{u}) \, \mathrm{d}\mathcal{B} + \int_{\mathcal{B}} g^2 \boldsymbol{\nabla}\boldsymbol{\sigma} \vdots \boldsymbol{\nabla}\boldsymbol{\varepsilon}(\delta \boldsymbol{u}) \, \mathrm{d}\mathcal{B}, \tag{8}$$

where superscript g refers to to the gradient-elastic modulus as a parameter.

An additional gradient parameter introducing a micro-inertia term has been proposed[51] in order to achieve a physically satisfactory dispersion relation for a large range of wave numbers[22]. The variation of the kinetic energy is then written in the form ([51]; Eq. (3.3) and (2.4) with (10.2))

$$\delta \int_T W^{\gamma}_{\text{kin}} \, \mathrm{d}\tau = -\int_T \Big(\int_{\mathcal{B}} \rho \ddot{\boldsymbol{u}} \cdot \delta \boldsymbol{u} \, \mathrm{d}\mathcal{B} + \int_{\mathcal{B}} \gamma^2 \rho \boldsymbol{\nabla}\ddot{\boldsymbol{u}} : \boldsymbol{\nabla}\delta \boldsymbol{u} \, \mathrm{d}\mathcal{B} \Big) \, \mathrm{d}\tau, \tag{9}$$

with T and ρ denoting a time interval of the time variable τ and mass density, respectively, and finally upper dot denoting the time derivative and γ standing for the micro-inertia parameter.

General energy expressions for external loadings (see[18,64,65]) are omitted here, the chosen assumptions for the beam bending problem are detailed in the next subsection.

Gradient-elastic Euler–Bernoulli beam models

Let us consider a three-dimensional beam structure

$$\mathcal{B} = A \times \Omega, \tag{10}$$

where $\Omega = (0, L)$ denotes the central axis of the structure with L standing for the length of the structure. A Cartesian coordinate system will be fixed to the structure such that the central axis follows the x-axis. Accordingly, $A = A(x) \subset \mathbb{R}^2$ denotes the cross section of the structure, with $\mathrm{diam}(A) \ll L$.

First of all, let us assume that the material properties and cross section of the beam as well as surface and body loads and (both static and kinematic) boundary conditions on the end point cross sections are of such a form that they allow us to focus on *uni-axial bending* in the xz-plane with displacement field $\boldsymbol{u} = (u_x, u_z)$. Within these assumptions, the dimension reduction hypotheses of the Euler–Bernoulli beam bending model imply the displacement components of the form

$$u_x = -z\frac{\partial w(x)}{\partial x}, \quad u_z = w(x), \tag{11}$$

in the global Cartesian (x, y, z) coordinate system – leaving the transverse deflection $w : \Omega \to \mathbb{R}$ as the only independent unknown of the problem.

The only non-zero strain component of the linear strain tensor (3) is now the axial strain $\epsilon_x = -z\partial^2 w/\partial x^2$ giving (8) in the form[40]

$$\begin{aligned}\delta W^g_{\text{int}} &= \int_0^L \int_A \sigma_x \epsilon_x(\delta u_x)\,\mathrm{d}A\,\mathrm{d}x + \int_0^L \int_A g^2 \nabla\sigma_x \cdot \nabla\epsilon_x(\delta u_x)\,\mathrm{d}A\,\mathrm{d}x \\ &= -\int_0^L \int_A \left(\sigma_x z + g^2\frac{\partial \sigma_x}{\partial z}\right)\mathrm{d}A\,\frac{\partial^2 \delta w}{\partial x^2}\,\mathrm{d}x - \int_0^L \int_A g^2 \frac{\partial \sigma_x}{\partial x} z\,\mathrm{d}A\,\frac{\partial^3 \delta w}{\partial x^3}\,\mathrm{d}x.\end{aligned} \tag{12}$$

Writing the curvature of the beam axis as

$$\kappa(w) = -\frac{\partial^2 w}{\partial x^2}, \tag{13}$$

with notation $\delta\kappa = \kappa(\delta w)$, and defining the force resultants, the classical Cauchy type bending moment and a generalized moment (called couple bending moment in[41]), respectively, as

$$M(x) = \int_A \sigma_x(x, y, z) z\,\mathrm{d}A, \quad R(x) = \int_A \frac{\partial \sigma_x(x, y, z)}{\partial z}\,\mathrm{d}A, \tag{14}$$

results in an energy expression over the central axis as

$$\delta W^g_{\text{int}} = \int_0^L (M + g^2 R)\delta\kappa\,\mathrm{d}x + \int_0^L g^2 \frac{\partial M}{\partial x}\frac{\partial \delta\kappa}{\partial x}\,\mathrm{d}x, \tag{15}$$

where we have assumed that the cross-sectional area is constant (cf. (12) and (15)) and $g = g(x)$. Integration by parts in (15) proposes defining the bending moment of the gradient-elastic model, or the total bending moment, as

$$M^g = M + g^2 R - \frac{\partial}{\partial x}\big(g^2 \frac{\partial M}{\partial x}\big), \tag{16}$$

which reduces to $M^g = M - g^2 M'' + g^2 R$ for constant g. Here and in what follows, prime denotes the x-derivative.

In what follows, we assume, for simplicity, that the material follows the Hooke's law in the form $\sigma_x = E\epsilon_x$ with Young's modulus E (assumed to be constant above) giving the bending moments as

$$M(x) = -\int_A E z^2 \frac{\partial^2 w}{\partial x^2}\,\mathrm{d}A = -EI\frac{\partial^2 w}{\partial x^2}, \tag{17}$$

$$R(x) = -\int_A \frac{\partial}{\partial z}(Ez\frac{\partial^2 w}{\partial x^2})\,\mathrm{d}A = -EA\frac{\partial^2 w}{\partial x^2}, \tag{18}$$

where I denotes the moment of inertia and is assumed to be constant, for simplicity. Finally, the internal virtual work expression takes the displacement form

$$\delta W^g_{\text{int}} = \int_0^L (EI + g^2 EA)\frac{\partial^2 w}{\partial x^2}\frac{\partial^2 \delta w}{\partial x^2}\,\mathrm{d}x + \int_0^L g^2 EI \frac{\partial^3 w}{\partial x^3}\frac{\partial^3 \delta w}{\partial x^3}\,\mathrm{d}x. \tag{19}$$

Remark 1. We note that the Poisson effect can be easily taken into account by adopting the generalized Hooke's law in (4) (see [34,39,41,66]).

Remark 2. In[30], the gradient operators in (15) have been reduced to the x-derivative (as addressed in[40]) which drops the generalized moment R from the energy expression leading to a reduced form

$$\begin{aligned}\delta W^g_{\text{int}} &= \int_0^L M\delta\kappa\,\mathrm{d}x + \int_0^L g^2 \frac{\partial M}{\partial x}\frac{\partial \delta\kappa}{\partial x}\,\mathrm{d}x \\ &= \int_0^L EI\frac{\partial^2 w}{\partial x^2}\frac{\partial^2 \delta w}{\partial x^2}\,\mathrm{d}x + \int_0^L g^2 EI\frac{\partial^3 w}{\partial x^3}\frac{\partial^3 \delta w}{\partial x^3}\,\mathrm{d}x.\end{aligned} \tag{20}$$

From the modeling point of view, this model can be justified in the energy sense by assuming that $g^2 EA \ll EI$. For a rectangular cross section (with thickness $t \ll L$), for instance, it should hold that $12g^2/t^2 \ll 1$ (see Sections 3 and 5 for further discussion on stiffening effects and model comparisons, and[67] (Section 9.1) for a reasoning considering the equilibrium of traction forces).

Regarding body load $\boldsymbol{f} : \mathcal{B} \to \mathbb{R}$ and surface load $\boldsymbol{g} : \mathcal{S} \to \mathbb{R}$, we assume that a transversal body loading $f_z = f_z(x, y, z)$ (even in z for exciting a bending state) is present and a transversal surface traction $g_z(x, y)$ acts on the appropriately defined upper and lower surfaces $\mathcal{S}_\pm$ of the beam at $z = \pm t/2$, together with axial surface

tractions $g_x(x,y)$ at $z=t/2$ and $-g_x(x,y)$ at $z=-t/2$ (all satisfying the bending state assumption). Accordingly, the external virtual work is written as

$$\delta W^0_{\text{ext}} = \int_{\mathcal{B}} \boldsymbol{f}\cdot\delta\boldsymbol{u}\,\mathrm{d}\mathcal{B} + \int_{\mathcal{S}_\pm} \boldsymbol{g}\cdot\delta\boldsymbol{u}\,\mathrm{d}\mathcal{S} = \int_0^L f\delta w\,\mathrm{d}x, \tag{21}$$

with load resultant

$$\begin{aligned} f(x) &= \int_A f_z\,\mathrm{d}A + 2\int_0^b g_z\,\mathrm{d}y + \frac{\partial}{\partial x}\int_0^b g_x\,t\,\mathrm{d}y \\ &= Af_z(x) + 2bg_z(x) + btg_x'(x), \end{aligned} \tag{22}$$

where b denotes the width of the beam in the y-direction and we have finally assumed that f_z is independent of y and z, g_z and g_x are independent of y and t is constant. For simplicity, we omit more general loading components for which the energy expressions can be derived by following the procedure introduced for Kirchhoff plates in [18].

Finally, for kinetic bending energy, dimension reduction results in

$$\begin{aligned} \delta\int_T W^\gamma_{\text{kin}}\,\mathrm{d}\tau = -\int_T \Big(\int_\Omega \rho\big(A\ddot{w}\,\delta w + I\ddot{w}'\,\delta w'\big)\,\mathrm{d}\Omega \\ + \int_\Omega \gamma^2\rho\big(2A\ddot{w}'\,\delta w' + I\ddot{w}''\,\delta w''\big)\,\mathrm{d}\Omega\Big)\,\mathrm{d}\tau, \end{aligned} \tag{23}$$

where both x- and z-components of the gradient have been included.

3. General boundary conditions and governing equations

In this section, the principle of virtual work, or Hamilton's principle, is applied for deriving the governing equations and the corresponding sets of boundary conditions. In particular, the gradient parameter is allowed to be non-constant and the boundary conditions are stated in terms of Cauchy force quantities, which provides a natural comparison to their classical counterparts.

First, integration by parts is applied in (15) giving

$$\delta W^g_{\text{int}} = \int_0^L (M + g^2R - (g^2M')')\delta\kappa\,\mathrm{d}x + [g^2M'\delta\kappa]_0^L, \tag{24}$$

which, by substituting $\delta\kappa = -(\delta w)''$ and integrating by parts twice, gives

$$\begin{aligned} \delta W^g_{\text{int}} = &-\int_0^L (M + g^2R - (g^2M')')''\delta w\,\mathrm{d}x + [(M + g^2R - (g^2M')')'\delta w]_0^L \\ &- [(M + g^2R - (g^2M')')(\delta w)']_0^L - [g^2M'(\delta w)'']_0^L. \end{aligned} \tag{25}$$

Now, the energy balance of the internal and external virtual works (15) and (21), respectively, gives the governing equation of the problem in terms of the bending

moments as

$$(M + g^2 R - (g^2 M')')'' = f \quad \text{in } \Omega, \tag{26}$$

or shortly $(M^g)' = f$ according to (16), and can be naturally written in terms of deflection according to (17) as

$$\big((EI + g^2 EA)w'' - (g^2 EIw''')'\big)'' = f. \quad \text{in } \Omega. \tag{27}$$

With constant material parameters, this reduces to $(EI + g^2 EA)w^{(4)} - g^2 EIw^{(6)} = f$ (cf. equation (23) in[40]). According to (26) and (16), the total shear force is of the form

$$Q^g = (M^g)' = (M + g^2 R - (g^2 M')')' \tag{28}$$

reducing to $Q^g = Q - g^2 Q'' + g^2 R'$ for constant g with $Q = M'$ denoting the standard Cauchy shear force.

Remark 3. Ignoring the z-derivative in the gradient term (see the physical reasoning in Remark 2) leads to a reduced governing equation of the form (cf. equation (11) in[30] derived for constant material parameters)

$$(M - g^2 M'')'' = f \quad \text{or} \quad (EIw'' - (g^2 EIw''')')'' = f \quad \text{in } \Omega. \tag{29}$$

From the mathematical point of view, however, the presence of the sixth-order derivative makes the most significant difference to the classical beam equation which follows from both (26) (or (27)) and (29) by setting $g = 0$.

For vibration problems, the governing equation (27) takes the form

$$\big((EI + g^2 EA)w'' - (g^2 EIw''')'\big)'' + \rho A(\ddot{w} - 2\gamma^2 \ddot{w}'') - \rho I(\ddot{w}'' - \gamma^2 \ddot{w}'''') = f \quad \text{in } \Omega, \tag{30}$$

where the last two terms in the left hand side (multiplied by ρI) represent the so-called rotatory inertia terms. It should be noticed that the term with factor 2 (multiplied by ρA) originates from the energy expression related to the x-derivative of δu_z and the z-derivative of δu_x.

Remark 4. The rotatory inertia terms are typically ignored (as in the examples of[22]) as higher order terms ($I \sim bt^3 \ll bt \sim A$ for small t). However, in the strain gradient models they are crucial for obtaining physical dispersion relation as noted in[67] and demonstrated in Section 6.

The boundary conditions, both essential and natural ones, corresponding to (26) are implied by the balance of virtual works in the following form:

$$w = \overline{w} \quad \text{or} \quad (M + g^2 R - (g^2 M')')' = \overline{Q}^g \quad \text{on } \partial\Omega, \tag{31}$$

$$w' = \overline{\beta} \quad \text{or} \quad (M + g^2 R - (g^2 M')') = \overline{M}^g \quad \text{on } \partial\Omega, \tag{32}$$

$$-w'' = \overline{\kappa} \quad \text{or} \quad g^2 M' = \overline{G}^g \quad \text{on } \partial\Omega. \tag{33}$$

The overlines denote prescribed boundary variables: deflection $\overline{w}$ and normal rotation $\overline{\beta}$ and their conjugate quantities, shear force $\overline{Q}^g$ and bending moment $\overline{M}^g$, are already present in the classical case with $g = 0$ as $\overline{V}$ and $\overline{M}$, respectively. In the current gradient-elastic model, however, additional given boundary quantities, curvature $\overline{\kappa}$ and its conjugate variable, double bending moment $\overline{G}^g$, appear.

From the physical point of view, the boundary conditions above should be now grouped such that they describe at least the three standard types: clamped, simply supported and free. Let us follow [18,56] and distinguish the clamped and simply supported boundaries into two different types according to the curvature: *singly* and *doubly* refering to unprescribed and prescribed curvature, respectively – with subscripts s and d, respectively. In this way, five different boundary condition types can be defined: *doubly clamped* and *singly clamped* boundaries, respectively,

$$w = \overline{w} \;\text{ and }\; w' = \overline{\beta} \;\text{ and }\; -w'' = \overline{\kappa} \quad \text{on } \Gamma_{\mathrm{C_d}}, \tag{34}$$

$$w = \overline{w} \;\text{ and }\; w' = \overline{\beta} \;\text{ and }\; g^2 M' = \overline{G}^g \quad \text{on } \Gamma_{\mathrm{C_s}}, \tag{35}$$

doubly simply supported and *singly simply supported* boundaries, respectively,

$$w = \overline{w} \;\text{ and }\; (M + g^2 R - (g^2 M')') = \overline{M}^g \;\text{ and }\; -w'' = \overline{\kappa} \;\text{ on } \Gamma_{\mathrm{S_d}}, \tag{36}$$

$$w = \overline{w} \;\text{ and }\; (M + g^2 R - (g^2 M')') = \overline{M}^g \;\text{ and }\; g^2 M' = \overline{G}^g \;\text{ on } \Gamma_{\mathrm{S_s}}, \tag{37}$$

and *free* boundaries,

$$\begin{aligned} (M + g^2 R - (g^2 M')')' &= \overline{Q}^g \;\text{ and} \\ (M + g^2 R - (g^2 M')') &= \overline{M}^g \;\text{ and} \\ g^2 M' &= \overline{G}^g \;\text{ on } \Gamma_{\mathrm{F}}, \end{aligned} \tag{38}$$

where $B = g^2 M'$ can be considered as a beam counterpart to the so-called surface stresses encountered within the corresponding three-dimensional strain gradient continuum [67]. Finally, we note that setting $g = 0$ results in the classical boundary conditions of Euler–Bernoulli beams.

In principle, one could even call (38) *doubly free* and introduce *singly free* as a boundary on which the curvature alone would be prescribed, which is not considered important here, however.

4. Variational formulation, solvability and Galerkin methods

In this section, the beam bending problem is first formulated in a variational form of a functional-analytic setting enabling to prove the solvability of the problem by continuity and ellipticity of the associated bilinear form. Error estimates for Galerkin discretizations follow as a natural consequence.

In what follows, we use notation $L^2(\Omega)$ for square-integrable real-valued functions defined on Ω and $H^s(\Omega)$ for a real Sobolev space of order s consisting of square-integrable real-valued functions defined on Ω with square integrable weak derivatives

up to order s. The corresponding Sobolev norm is denoted by $||\cdot||_s$ and the seminorm by $|\cdot|_s$.

The following variational formulations correspond to energy expressions (19) and (20) – entitled as the *full strain gradient* model and the *reduced strain gradient* model, respectively:

Problem 1. *For $f \in L^2(\Omega)$, find $w \in W \subset H^3(\Omega)$ such that*

$$a(w,v) = l(v) \quad \forall v \in V \subset H^3(\Omega), \tag{39}$$

where the bilinear form $a : W \times V \to \mathbb{R}$, $a(w,v) = a^c(w,v) + a^\nabla(w,v)$, and the load functional $l : V \to \mathbb{R}$, respectively, are defined as

$$a^c(w,v) = \int_\Omega EIw''v'' \,\mathrm{d}\Omega, \tag{40}$$

$$a^\nabla(w,v) = \int_\Omega g^2 EAw''v'' \,\mathrm{d}\Omega + \int_\Omega g^2 E(Iw'')'v''' \,\mathrm{d}\Omega, \tag{41}$$

$$l(v) = \int_\Omega f\, v \,\mathrm{d}\Omega. \tag{42}$$

The trial function set

$$W = \{v \in H^3(\Omega) \;\mid\; v_{|\Gamma_\mathrm{S}\cup\Gamma_\mathrm{C}} = \bar{w},\; v'_{|\Gamma_\mathrm{C}} = \bar{\beta},\; -v''_{|\Gamma_{\mathrm{C_d}}\cup\Gamma_{\mathrm{S_d}}} = \bar{\kappa}\} \tag{43}$$

consists of functions satisfying the essential boundary conditions, with given Dirichlet data $\bar{w}, \bar{\beta}, \bar{\kappa}$, whereas test function space V consists of H^3 functions with the corresponding homogeneous Dirichlet boundary conditions.

Problem 2. *For $f \in L^2(\Omega)$, find $w \in W \subset H^3(\Omega)$ such that*

$$a(w,v) = l(v) \quad \forall v \in V \subset H^3(\Omega), \tag{44}$$

where the bilinear form $a^\nabla(\cdot,\cdot)$ of Problem 1 is redefined as

$$a^\nabla(w,v) = \int_\Omega g^2 E(Iw'')'v''' \,\mathrm{d}\Omega, \tag{45}$$

whereas other notation remains unchanged.

Remark 5. The bilinear form of Problem 2 is form-identical to the weak form of the single-variable locking-free formulation for the classical Timoshenko beam model introduced in[57] (cf. equation (35)): the bending displacement w_b of[57] can be identified with deflection w, whereas ratio K_b/K_s of bending stiffness K_b and shear stiffness K_s can be identified with g^2. Therefore, the following theoretical analysis can be extended to the variational formulation of[57] as well.

The energy norm induced by the bilinear form of Problem 1, defined as

$$\|v\|_a^2 = a(v,v) = \int_\Omega (EI + g^2 EA)(v'')^2 \,\mathrm{d}\Omega + \int_\Omega g^2 EI (v''')^2 \,\mathrm{d}\Omega, \tag{46}$$

for constant bending stiffness EI, is equivalent to the H^3-norm whenever $W = V$, which can be seen in the proofs below. In addition, the symmetry of the bilinear form is clearly guaranteed: $a(u,v) = a(v,u)\ \forall u, v \in V$. For Problem 2, the energy norm reduces to the form

$$\|v\|_a^2 = a(v,v) = \int_\Omega EI (v'')^2 \,\mathrm{d}\Omega + \int_\Omega g^2 EI (v''')^2 \,\mathrm{d}\Omega. \tag{47}$$

In the limit case $g = 0$, both bilinear forms reduce to the classical one $a^{\mathrm{c}}(\cdot,\cdot)$ of H^2-regular functions.

The continuity and ellipticity of the bilinear form – for each positive g – guarantee the well-posedness of the problem. For simplicity, the proof is provided here for constant material values and fully clamped beams with $\partial\Omega = \Gamma_{\mathrm{C_s}}$ and $W = V$.

Theorem 1. *Let us assume that $\partial\Omega = \Gamma_{\mathrm{C_s}}$ and $W = V$. For any g, there exists a positive constant $C = C(g)$ such that*

$$a(u,v) \leq C\|u\|_3\|v\|_3 \quad \forall u, v \in V. \tag{48}$$

Proof. First, for the classical part the elementary proof of the one-dimensional Cauchy–Schwartz inequality gives the bound

$$a^{\mathrm{c}}(u,v) \leq EI|u|_2|v|_2.$$

In an analogous way, for the non-classical part (of Problem 1) it holds that

$$a^{\nabla}(u,v) \leq g^2 EA|u|_2|v|_2 + g^2 EI|u|_3|v|_3, \tag{49}$$

for constant bending stiffness EI. Altogether, we get the upper bound

$$a(u,v) \leq (EI + g^2 EA)|u|_2|v|_2 + g^2 EI|u|_3|v|_3 \leq C\|u\|_3\|v\|_3,$$

where $C = EI + g^2(EA + EI)$ reduces to $C = EI(1 + g^2)$ for Problem 2. This guarantees the continuity of the bilinear form $a(\cdot,\cdot)$ with respect to the H^3-norm.

Theorem 2. *Let us assume that $\partial\Omega = \Gamma_{\mathrm{C_s}}$ and $W = V$. For any $g > 0$, there exists a positive constant $\alpha = \alpha(g)$ such that*

$$a(v,v) \geq \alpha\|v\|_3^2 \quad \forall v \in V. \tag{50}$$

Proof. First, for the classical part we recall the elementary one-dimensional Poincaré–Friedrichs inequality in order to keep track on the constants involved in the analysis. With $v(0) = 0$, the fundamental theorem of calculus and the Cauchy–Schwartz inequality

imply that

$$\|v\|_0^2 \leq L^2 |v|_1^2. \tag{51}$$

Hence, $\|v\|_1^2 \leq (1+L^2)|v|_1^2$. In an analogous way, with $v'(0)=0$, it holds that $|v|_1^2 \leq L^2|v|_2^2$ and hence it holds that $\|v\|_2^2 \leq (1+L^2+L^4)|v|_2^2$ implying the bound

$$a^{\mathrm{c}}(v,v) = EI|v|_2^2 \geq \frac{EI}{1+L^2+L^4}\|v\|_2^2. \tag{52}$$

Second, for the non-classical part it trivially holds that

$$a^{\nabla}(v,v) = g^2 EA|v|_2^2 + g^2 EI|v|_3^2, \tag{53}$$

which gives (for Problem 1) the lower bound

$$a(v,v) \geq \frac{EI+g^2EA}{1+L^2+L^4}\|v\|_2^2 + g^2 EI|v|_3^2 \geq \alpha\|v\|_3^2. \tag{54}$$

where $\alpha = \min((EI+g^2EA)/(1+L^2+L^4), g^2EI)$ reduces to $\alpha = EI\min((1+L^2+L^4)^{-1}, g^2)$ for Problem 2. This quarantees that the bilinear form $a(\cdot,\cdot)$ is elliptic over space V endowed with the H^3-norm.

According to Riesz Representation Thorem, the gradient-elastic Euler–Bernoulli beam problem with fully clamped boundaries has a unique solution:

Theorem 3. *Let us assume that $\partial\Omega = \Gamma_{\mathrm{C_s}}$, $W = V$ and $g > 0$. For a given loading $f \in L^2(\Omega)$, Problems 1 and 2 have unique solutions in V.*

Proof. By continuity and ellipticity, the bilinear form $a(\cdot,\cdot)$ is an inner product on V and hence the pair $(V, a(\cdot,\cdot))$ is a Hilbert space. In addition, by the Cauchy–Schwartz inequality the load functional $l(\cdot)$ belonging to the dual space V' is linear and continuous on V:

$$l(v) = \int_\Omega f\, v \,\mathrm{d}\Omega \leq \|f\|_0\|v\|_3 \quad \forall v \in V. \tag{55}$$

Riesz Representation Thorem implies unique solutions for Problems 1 and 2.

For free bending vibrations of the beam problem, the inertia terms corresponding to (30) are of the form (cf. (23))

$$m^{\mathrm{c}}(w,v) = \int_\Omega \rho A\ddot{w}\, v \,\mathrm{d}\Omega + \int_\Omega \rho I\ddot{w}'\, v' \,\mathrm{d}\Omega, \tag{56}$$

$$m^{\nabla}(w,v) = \int_\Omega 2\gamma^2\rho A\ddot{w}'v' \,\mathrm{d}\Omega + \int_\Omega \gamma^2\rho I\ddot{w}''v'' \,\mathrm{d}\Omega. \tag{57}$$

Let us solve Problems 1 and 2 by conforming Galerkin methods giving approximation w_h converging to the exact solution w with grid size h:

Method 1. *For $f \in L^2(\Omega)$, find $w_h \in W_h \subset W$ such that*

$$a(w_h, v) = l(v) \quad \forall v \in V_h \subset V. \tag{58}$$

With the conformity of the method, i.e., $V_h \subset V$, requiring C^2-continuous basis functions, the continuity and ellipticity of the continuous problem are inherited by the discrete problem. This implies the following error estimates which can be proved in a standard way by imitating the steps for proving the so-called Cea's lemma[68] (first, use ellipticity; second, use Galerkin orthogonality implied by conformity and consistency; third, use continuity):

Proposition 1. *Let us assume that $\partial\Omega = \Gamma_{C_s}$, $W = V$ and $g > 0$. For a given loading $f \in L^2(\Omega)$, it holds that*

$$\|w - w_h\|_3 \leq \frac{C}{\alpha} \inf_{0 \neq v \in V_h} \|w - v\|_3. \tag{59}$$

Approximation properties of B-splines or the corresponding classical ones for polynomials imply a more quantitative error estimate in terms of basis function order p and mesh size h:

Corollary 1. *With the assumptions of Proposition 1, it holds that*

$$\|w - w_h\|_3 \leq \frac{C}{\alpha} c h^{p-2} |w|_{p+1}. \tag{60}$$

where the exact solution of the problem is assumed to be smooth enough, i.e., $w \in H^{p+1}(\Omega)$, and interpolation constant c is independent on w and h.

Finally, we note that since constants C and α depend on g the error estimates depend on g as well. However, numerical results in Section 6 show that convergence results are very good for a wide range of parameter values. Due to boundary layers of the solution, in turn, regularity assumption $w \in H^{p+1}(\Omega)$ might not be realistic for large values of p. Numerical examples of boundary layers are given in Section 6.

5. Model comparisons

This section is devoted to a model comparison between the two strain gradient beam models of the previous sections (Problems 1 and 2; cf.[40,41] and[30]) and other two beam models based on modified strain gradient and couple stress theories ([34] and[38,39]) – and the corresponding classical beam model. In particular, the comparison reveals that our variational analysis is extendable to the other two generalized beam models, and that the generalized beam models demonstrate two different kinds of parameter-dependent stiffening behavior – one of these kinds (possessed by three models out of four) provides capturing experimental results.

Formulations for modified strain gradient and couple stress models

Let us consider Mindlin's strain gradient elasticity theory of form I[51] giving strain energy density (equation (9.11) in[51]; cf. (1))

$$\begin{aligned}\mathcal{W}_I = &\frac{1}{2}\lambda\varepsilon_{ii}\varepsilon_{jj} + \mu\varepsilon_{ij}\varepsilon_{ij} + a_1\eta_{iik}\eta_{kjj} + a_2\eta_{ijj}\eta_{ikk} \\ &+ a_3\eta_{iik}\eta_{jjk} + a_4\eta_{ijk}\eta_{ijk} + a_5\eta_{ijk}\eta_{kji},\end{aligned} \tag{61}$$

where the (third-order) micro-deformation tensor is defined by the second gradient of the displacement as (cf. (2))

$$\boldsymbol{\eta} = \boldsymbol{\nabla}\boldsymbol{u}. \tag{62}$$

The work conjugate (third-order) double stress tensor is now defined by a set of five non-classical material parameters $a_1 = a_1(x, y, z), ..., a_5 = a_5(x, y, z)$ ($\tilde{a}_i$ in Mindlin's notation) as $\tau_{ijk} = \partial\mathcal{W}_I/\partial\eta_{ijk} = \tau_{jik}$.

Within the modified version proposed in[24], the strain energy density is written as (cf. (6))

$$\mathcal{W}_I = \frac{1}{2}\lambda\varepsilon_{ii}\varepsilon_{jj} + \mu\varepsilon_{ij}\varepsilon_{ij} + l_0\varepsilon_{mm,i}\varepsilon_{nn,j} + l_1\gamma^{(1)}_{ijk}\gamma^{(1)}_{ijk} + l_2\chi^{\mathrm{s}}_{ij}\chi^{\mathrm{s}}_{ij}, \tag{63}$$

with three length scale parameters l_0, l_1 and l_2 associated to the dilatation gradients, deviatoric stretch gradients and symmetric parts of rotation gradients, respectively. The last two are defined as follows: $\gamma^{(1)}_{ijk} = \gamma^{\mathrm{s}}_{ijk} - (\delta_{ij}\gamma^{\mathrm{s}}_{mmk} + \delta_{jk}\gamma^{\mathrm{s}}_{mmi} + \delta_{ij}\gamma^{\mathrm{s}}_{mmj})/5$ with $\gamma^{\mathrm{s}}_{ijk} = (u_{i,jk} + u_{j,ki} + u_{k,ij})/3$ and $\chi^{\mathrm{s}}_{ij} = (\chi_{ij} + \chi_{ij})/2$ with $\chi_{ij} = e_{imn}\gamma_{jmn} = e_{imn}u_{n,jm}$. Without giving further details, we simply recall that for the Euler–Bernoulli beam problem this modification leads to a sixth-order governing equation ((21) in[39] with a simplyfying assumption $\nu = 0$):

$$\big(EI + EA(l_0^2 + \frac{4l_1^2}{15} + \frac{l_2^2}{2})\big)w^{(4)} - EI\big(l_0^2 + \frac{2l_1^2}{5}\big)w^{(6)} = f, \tag{64}$$

with boundary conditions very similar to the ones presented in (34)–(38). This differential equation is clearly form-equivalent to equation (27).

The corresponding bilinear form can be obtained by identifying the terms in energy expression (13) of[39] with the gradient part of the bilinear form of Problem 1 (by assuming constant material parameters, for simplicity):

$$a^{\nabla}(w, v) = \int_\Omega EA\big(l_0^2 + \frac{4l_1^2}{15} + \frac{l_2^2}{2}\big)w''v''\,\mathrm{d}\Omega + \int_\Omega EI\big(l_0^2 + \frac{2l_1^2}{5}\big)w'''v'''\,\mathrm{d}\Omega. \tag{65}$$

The stability results for this formulation follow by modifying the corresponding steps of the proofs of Theorems 1 and 2.

Another closely related beam model has been introduced and analyzed in[34] by following a modified couple stress theory proposed by[35] . The strain energy density and

governing equation of the model can be, however, obtained as a special case of (63) and (64), respectively, by simply setting $l_0 = l_1 = 0$ giving a one-parameter model leading to a fourth-order governing equation, in particular ((26) in [34] with a simplyfying assumption $\nu = 0$):

$$\big(EI + EA\frac{l^2}{2})\big)w^{(4)} = f. \tag{66}$$

The corresponding bilinear form can be obtained by simply setting $a^{\nabla}(\cdot,\cdot) = 0$ in Problem 1 and then augmenting the classical H^2-part $a^c(\cdot,\cdot)$ by an l^2-dependent addendum, and finally modifying the energy norm accordingly. The stability results follow by modifying the steps corresponding to the classical parts of the proofs of Theorems 1 and 2. In this case, a $C^1(\Omega)$-continuous disretization (with Hermite shape functions, for instance) provides an $H^2(\Omega)$-conforming method (see Section 6.5). This model has been later extended in [36] by a surface energy term according to [37], which leads to including a second-order term in (66), essentially.

Model comparisons with a cantilever beam

In this subsection, we compare the four models presented above – full strain gradient (SG) model of Problem 1 [40,41], reduced strain gradient model of Problem 2 [30], modified strain gradient model [38,39] and modified couple stress (CS) model [34,36] – both to each other and to the classical Euler–Bernoulli beam model. For this purpose, we solve a problem of a transversely point-loaded cantilever beam by analytical means. The beam is clamped (singly clamped for the sixth-order models) at one end ($x = 0$) and a point load $\overline{Q}^g$ acts at the other end ($x = L$).

In order to clarify the essential differences of the solutions, we write the governing equation of the problem in a generic form (by assuming constant material parameters)

$$EI(c^g w^{(4)} - d^g w^{(6)}) = f, \tag{67}$$

with constants c^g and d^g specified below for each model ($c^g = 1$ and $d^g = 0$ for the classical beam model). First of all, we note that for a rectangular cross section, for instance, with the thickness $t \ll L$, it holds that $EA/EI = 12/t^2$, whereas for circular cross sections $EA/EI = 16/t^2$. Therefore, we use notation $EA/EI = \alpha/t^2$ with constant α depending on the cross section, in order to study the thickness dependence of the models.

For the full and reduced SG-models, constants c^g and d^g are determined, respectively, by (27) and (29) giving

$$d^g = g^2, \quad c^g = 1 + \alpha g^2/t^2 \quad \text{(full SG model)}, \tag{68}$$

$$d^g = g^2, \quad c^g = 1 \quad \text{(reduced SG model)}. \tag{69}$$

For the modified SG-model, setting $l_0 = l = l_1 = l_2$ in (64) implies that c^g and d^g are replaced by

$$d^l = dl^2, d = 7/5, \quad c^l = 1 + c\alpha l^2/t^2, c = 53/30 \quad \text{(modified SG)}. \tag{70}$$

For the modified CS-model, it holds that

$$d^l = 0, \quad c^l = 1 + c\alpha l^2/t^2, c = 1/2 \quad \text{(modified CS model)}. \tag{71}$$

Let us consider the maximum deflection at the free end of the beam denoted by w_L giving bending rigidity $D = \overline{Q}^g/w_L$ which for the classical beam model is of the form $D_0 = 3EI/L^3$.

First, for studying the differences of the reduced and full strain gradient models, the normalized bending rigidity D/D_0 (see the Appendix) is plotted against the thickness parameter t in Figure 1 (left), with $0 \leq t \leq 0.15L = 150$ μm, for two gradient parameter values, $g = 5$ μm (solid lines) and $g = 50$ μm (dashed lines) with a fixed length $L = 1000$ μm. As can be deduced from (69) and seen in the figure, the normalized bending rigidity of the reduced SG-model is independent of the thickness and very close to the classical value: for $g = 5$ μm (grey solid line) $D/D_0 = 1.000007$, whereas for $g = 50$ μm (black dashed line) $D/D_0 = 1.007$. This demonstrates the first kind of stiffening effect which stems from g^2 factoring the sixth-order term in (67). On the contrary, the normalized bending rigidity of the full SG-model increases dramatically with decreasing thickness values (red solid line for $g = 5$ μm and red dashed line for $g = 50$ μm). As indicated by (68) as well, this demonstrates the combination of the first and second kinds of stiffening effect; the second one stemming from g^2/t^2 factoring the fourth-order term. The modified SG-model (blue lines) shares the same feature (see (70)), whereas the modified CS-model (green lines) demonstrates the (almost invisible) second kind stiffening effect alone (cf. (71)).

Second, for comparing the stiffening behavior to experimental results taken from[24] (including a comparison to the modified SG model), the corresponding curves for the full SG model are plotted in Figure 1 (right) for $g = 4, 6.5$ (the best fit), $8, 10$ μm. As a conclusion, we can state that the second kind stiffening effect is qualitatively different and drastically stronger than the first kind effect and enables capturing the experimentally observed stiffening effect observed for the epoxy materials of the experiment (cf. the coresponding comparisons to experiments for the modified CS model in[26,34]).

Third, we compare the stiffening behavior of the full SG model to the experimental results taken from[27] studying elastic properties of silver nanowires with outer diameters ranging from 20 to 140 nm. In Figure 2, one can observe a clear diameter dependence in both the experimental results (black circles) and the fitting curve (black dashed line) based on a theoretical analysis for the size dependence of the "apparent Young's modulus" attributed to the surface effect, the oxidation layer and the surface roughness. Surprisingly, the stiffening behavior of the strain gradient model (red solid line) is quite close to the observed size dependence – although the fundamental physical reasonings for nano- and micro-scales are different and hence this comparison should be primarily taken as a demonstration of the similarity of the stiffening effects of these two scales.

6. Isogeometric implementation and numerical examples

In this section, we first introduce an isogeometric, C^2-continuous B-spline discretization of Method 1 and confirm the theoretical convergence results of Corollary 1 by studying

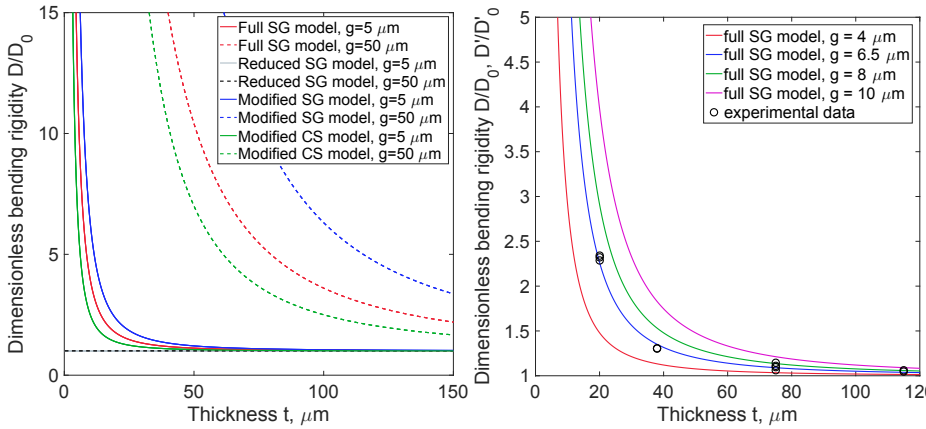

Figure 1. Singly clamped cantilever micro-beam: thickness dependence of bending rigidity D/D_0 for four different strain gradient models (left) and a comparison to experimental results (right).

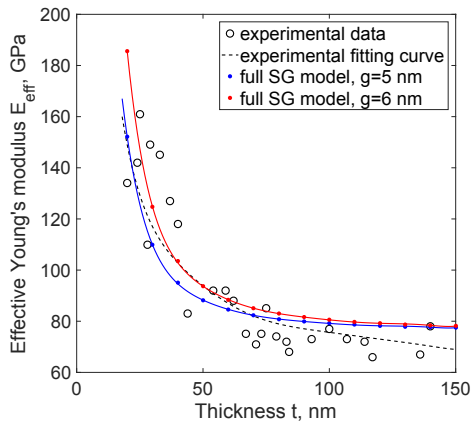

Figure 2. Singly simply supported nano-beam: effective experimental Young's modulus versus the thickness dependence of the bending rigidity.

numerical benchmark problems of statics with analytical exact solutions. Second, we illustrate some essential differences between the two model variants of strain gradient elasticity and the one of classical elasticity. Third, we study the accuracy of natural frequencies and eigenmodes provided by the numerical method.

Finally, we demonstrate the size dependency of the effective Young's modulus of an auxetic cellular metamaterial in which auxeticity is governed by bending-dominated deformation of cell struts, which is a typical fundamental feature for auxetic metamaterials relying on a cell architecture[8,9]. The struts are modelled by incorporating

the modified couple stress beam formulation into a commercial finite element software providing a C^1-continuous discretization for beam bending.

Isogeometric B-spline implementation

Method 1 has been implemented by using isogeometric discretizations[56,58,60,61,69]: Associated to an open knot vector $\{0 = x_1, \ldots, x_{n+p+1} = L\}$, with n denoting the number of basis functions and $L = 1$, B-splines of order $p \geq 1$ are defined recursively by Cox–de Boor recursion (by definition $0/0 = 0$) as

$$N_{i,p}(x) = \frac{x - x_i}{x_{i+p} - x_i} N_{i,p-1}(x) + \frac{x_{i+p+1} - x}{x_{i+p+1} - x_{i+1}} N_{i+1,p-1}(x), \tag{72}$$

where the zeroth order ones are defined as follows: $N_{i,0}(x) = 1$ for $x_i \leq x < x_{i+1}$ and $N_{i,0}(x) = 0$ elsewhere. For the corresponding approximation $w_h(x) = \sum_{i=1}^{n} N_{i,p}(x)\hat{w}_i$, with (unknown) control variables $\hat{w}_i$, these functions provide regularity C^{p-1} over the mesh. In particular, since $C^{p-1}(\Omega) \subset H^3(\Omega)$ with $p \geq 3$ this approach provides $H^3(\Omega)$-conforming discretizations for Problems 1 and 2.

Our implementation follows the standard Galerkin approach essentially described in[57] (Sections 3.1 and 3.2) giving the element stiffness matrix (for Problem 1 with I assumed to be constant) and force vector, respectively, as

$$\boldsymbol{K}_e = \int_e (EI + g^2 EA)\boldsymbol{N}''^T \boldsymbol{N}'' \,\mathrm{d}x + \int_e g^2 EI \boldsymbol{N}'''^T \boldsymbol{N}''' \,\mathrm{d}x, \tag{73}$$

$$\boldsymbol{f}_e = \int_e f\, \boldsymbol{N}^T \,\mathrm{d}x, \tag{74}$$

where $\boldsymbol{N}$ denotes, as usual, the row vector of the shape functions.

Convergence study of a singly simply supported beam

Let us consider a thin beam of a square cross section with thickness $t = L/20$, length $L = 1$ and Young's modulus $E = 210000$. Loading

$$f(x) = f_0 \mathrm{e}^{x/L} \tag{75}$$

is applied along the beam axis with $f_0 = 0.1/(EI)$. The analytical solution following the beam equation (27), with singly simply supported boundary conditions (37), can be written in the form

$$w(x) = c_0 + c_1 x + c_2 x^2 + c_3 x^3 + c_4 g^4 \sinh(x/g) + c_5 g^4 \cosh(x/g) + \frac{f_0 L^4}{EI(1 - g^2/L^2)} \mathrm{e}^{x/L}, \tag{76}$$

with constants c_i, $i = 0, ..., 5$ determined by the boundary conditions.

First, the convergence properties of the method are studied with respect to different norms for the gradient parameter value $g/L = 0.05 = t/L$. In Figure 3 (left), the relative

error in the H^3-norm is plotted against the mesh size (in logarithmic scales) for B-spline orders $p = 3, 4, 5$ with continuity C^{p-1}. Solid lines refer to the full SG-model, dashed lines refer to the reduced SG-model. It can be seen that the convergence rates fairly strictly follow the theoretical order $\mathcal{O}(h^{p-2})$ predicted by Corollary 1. It should be noticed that the H^3-norm (with third-order derivatives) measures the error in the bending energy (46).

Second, for studying the parameter dependence of the convergence rates (see the remark below Proposition 1), relative errors in the H^3-norm with $p = 3$ are plotted in Figure 3 (right), for three different values of the gradient parameter: $g/L = 0.1, 0.05, 0.035$. According to these plots, g does not affect the asymptotic convergence order as predicted by the theoretical results, whereas it slightly shifts the error level upwards: decreasing g increases the error.

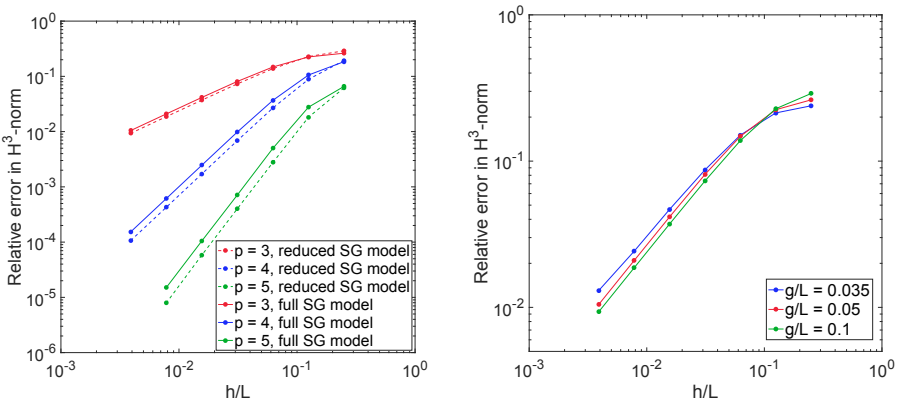

Figure 3. Singly simply supported beam: (left) Convergence in the H^3-norm for $p = 3, 4, 5$ with $g/L = 0.05$; (right) Convergence in the H^3-norm for $p = 3$ with $g/L = 0.1, 0.05, 0.035$.

Third, convergence rates for the relative error in lower-order norms (H^2, H^1 and L^2 with H^3 as a reference) are plotted in Figure 4 for orders $p = 4$ and 5 (left and right, respectively). It should be noticed that as for the classical beam model the H^1-norm measures the error in the rotation, whereas the H^2-norm measures the error in the Cauchy bending moment M or in the Cauchy part of the bending energy. For the H^2-norm, the convergence order is close to $\mathcal{O}(h^{p-1})$. There is a natural decrease in the error level and improvement in the convergence rate compared to the H^3-error. Analogous improvements hold for the H^1-norm as well. For the L^2-norm, these improvements are still clear but not that significant any more.

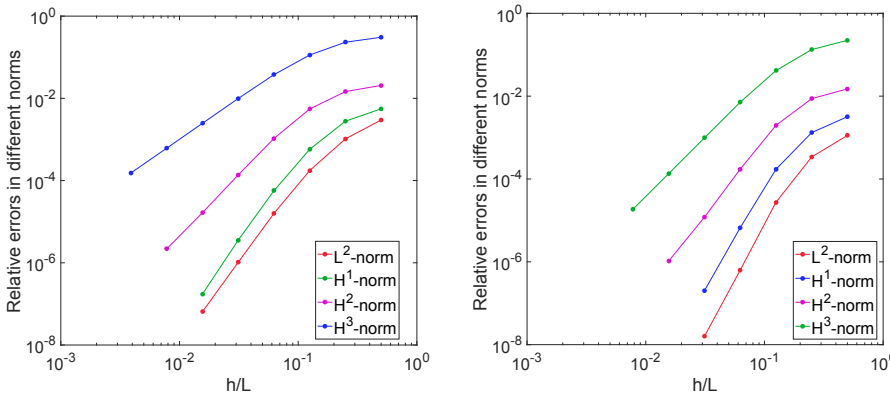

Figure 4. Singly simply supported beam: Convergence in the H^3, H^2, H^1 and L^2-norms for $p = 4$ (left) and $p = 5$ (right) with $g/L = 0.05$.

Parameter-dependent stiffening and boundary layers

In this subsection, we demonstrate and compare the parameter-dependent stiffening effect and boundary layers of the two variants of gradient-elastic Euler–Bernoulli beam models, the full and reduced SG-models.

First, we illustrate the distributions of the deflection for these two models; for the singly simply supported beam of Section 6.2 with $p = 5$ and 128 degrees of freedom. The deflection distributions in Figure 5, for three different values of the gradient parameter, $g/L = 0.1, 0.01, 0.001$, show that the deflection of the full SG-model (solid lines) distinctly depends on the gradient parameter, whereas for the reduced SG-model (dashed lines) the parameter dependence is diminutive. For the largest parameter value $g/L = 0.1$ (green dashed line), however, the reduced model shows a clear parameter dependence (stiffening) as well.

Second, we compare the deflection distributions of the models with different (extreme) values of ratio g/t (cf. condition $12g^2/t^2 \ll 1$ in Remark 2): with $g/L = 0.01$, the deflection distributions for $g/t = 1$ and $g/t = 0.2$ are plotted in Figures 6 (left and right, respectively). These plots show that decreasing ratio g/t essentially decreases the difference between the solutions of the models. In general, the full SG-model implies an essentially stiffer beam than the reduced SG-model (combining the first and second kind stiffening) which, in turn, gives a stiffer beam than the classical beam model (the first kind stiffening alone).

Third, in order to illustrate the boundary layers of the solutions – produced by the sixth-order term of (29) (or (27) for the full SG model) – we compare the bending moment and shear force of the reduced SG-model defined in (16) and (28), respectively, to the ones given by the classical beam model (with $g = 0$). In Figure 7 (left), the total moment M^g (dashed line), i.e., the moment corresponding to the total stress, and its classical part M, i.e., the moment corresponding to the Cauchy stress, are plotted along the beam axis for parameter values $g/L = 0.05, 0.02, 0.01, 0.005$ with $p = 5$. The corresponding

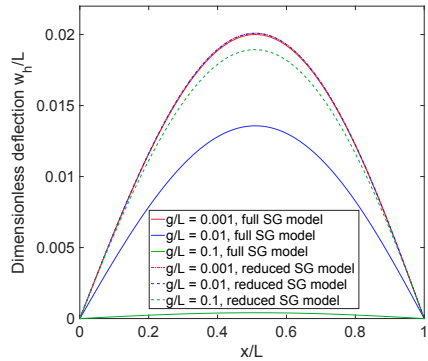

Figure 5. Singly simply supported beam: Deflection with $p = 5$ for $g/L = 0.1, 0.01, 0.001$.

shear forces are plotted in Figure 7 (right). These distributions reveal that the solution exhibits a boundary layer clearly visible in the classical part (solid lines), already evident from the hyperbolic functions (with argument x/g for small g) of the analytical solution for the deflection in (76). However, the boundary layer is not present in the (quadratic) total moment or in the (linear) total shear force (black dashed lines) which can be solved for this statically determined model problem from the second-order moment equation of (29).

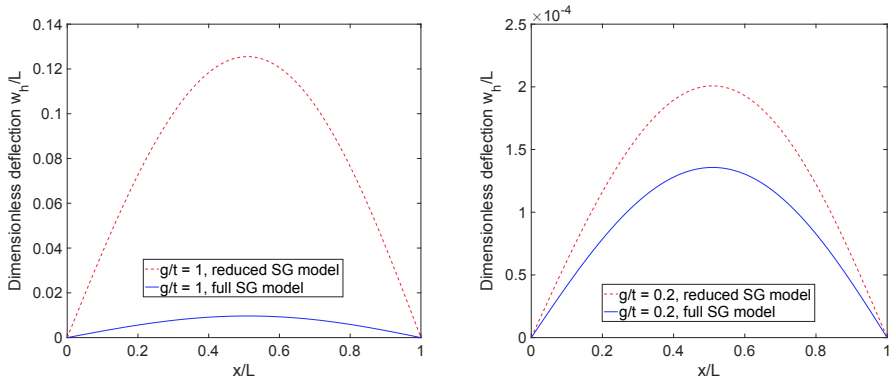

Figure 6. Singly simply supported beam: Deflection $p = 5$ with $g/L = 0.01$ for $g/t = 1$ (left) and $g/t = 0.2$ (right).

Finally, the deflection of another singly simply supported beam is studied with $L = 1$, $t/L = 0.02$ and with Young's modulus of silver. In Figure 8 (left), the location of the supports (at $x = 0$ and $x = L/2$) is depicted with the deflection curves for $g/L = 0.01, 0.005, 0.001$ with $p = 5$ and 20 elements demonstrating the parameter dependence. Different terms of the total bending moment (see (16)) are plotted in Figure 8 (right)

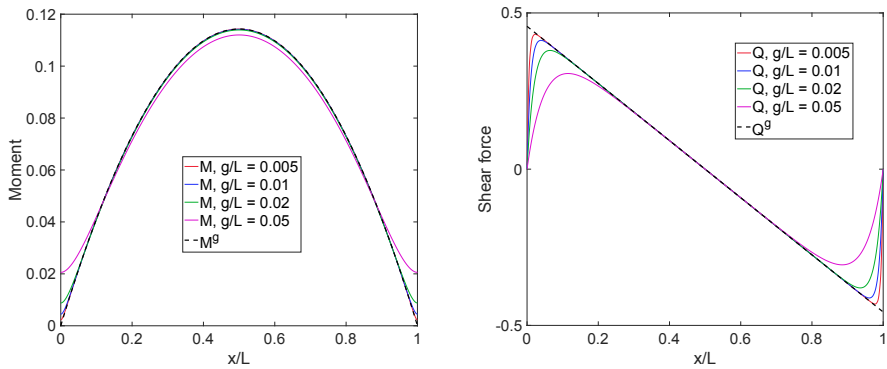

Figure 7. Singly simply supported beam: Moments M and M^g (left) and shear forces Q and Q^g (right) for $g/L = 0.05, 0.02, 0.01, 0.005$ with $p = 5$.

with the corresponding moment of the classical problem as a reference (M^0, black dashed line). Regarding the moment curves, it should be noticed that the due to the singly simple supports the exact total moment M^g (approximated by the magenta line of M_h^g) equals to the exact classical one M^0. Some of the curves are smooth since the deflection is even C^4-continuous. We note as well that the support at the middle of the beam is imposed by the standard penalization technique typically used in isogeometric methods (not necessarily providing degrees of freedom for nodal values due to the non-interpolatory nature of the approximation with respect to the internal nodes).

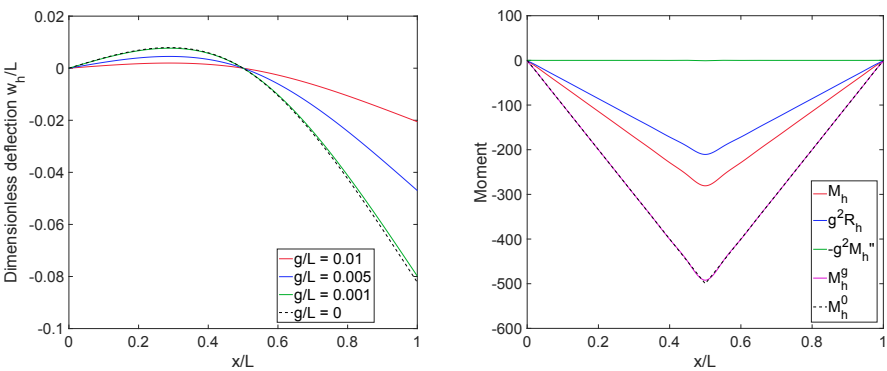

Figure 8. Singly simply supported cantilever beam: Deflection and bending moment for $g/L = 0.01, 0.005, 0.001$.

Free vibration study of a doubly simply supported beam

Let us next consider a doubly simply supported thin beam for which the full SG model following equation (30) gives natural frequencies

$$\omega_{g,\gamma}^2 = k^4 \frac{EI}{\rho A} \frac{1 + g^2 A/I + g^2 k^2}{1 + 2\gamma^2 k^2 + I(k^2 + \gamma^2 k^4)/A}, \quad k = \frac{\pi n}{L}. \tag{77}$$

The dimensionless phase velocity of the full SG model

$$\hat{v}_{g,\gamma} = \frac{v_{g,\gamma}}{v_c} = \sqrt{\frac{\hat{k}^2(1 + \alpha(g/t)^2) + \alpha(g/t)^2 \hat{k}^4}{1 + 2\alpha(\gamma/t)^2 \hat{k}^2 + \hat{k}^2 + \alpha(\gamma/t)^2 \hat{k}^4}}, \tag{78}$$

where $v_{g,\gamma} = \omega_{g,\gamma}/k$ and $v_c = \sqrt{E/\rho}$, is plotted in Figure 9 (left, green line) as a function of the dimensionless wave number $\hat{k} = k\sqrt{I/A}$ with $g/L = 0.01$ and $\gamma/L = 0.005$. The corresponding quantity for the reduced SG model is plotted in the same figure (blue line). Furthermore, it can be noticed in the same figure, as already addressed in [67], that including the rotatory terms for beams (not $\gamma \neq 0$ alone as for strain gradient models in general; see [22]) guarantees avoiding non-physical dispersion curves tending to infinity (red and magenta lines), meaning unbounded wave velocities for very high wavenumbers (or frequencies).

Second, in Figure 9 (right), the relative error in the H^3-norm for the fifth eigenmode with $g/L = 0.1 = \gamma/L$ is plotted against the mesh size (in logarithmic scales) for B-spline orders $p = 3, 4, 5, 6$ with continuity C^{p-1}. The results show that the convergence rates quite systematically follow order $\mathcal{O}(h^{p-1})$.

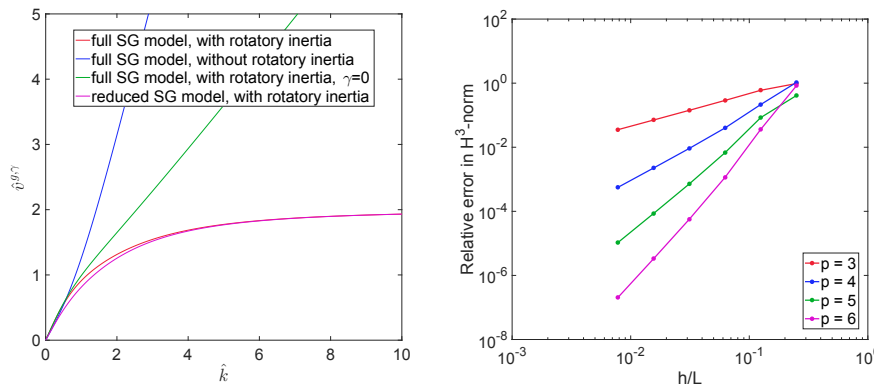

Figure 9. Doubly simply supported beam: (left) Dispersion curves with $p = 5$ for different combinations of parameters g and γ; (right) Convergence of the fifth eigenmode in the H^3-norm for $p = 3, 4, 5$ and 6 with $g/L = 0.1 = \gamma$.

Third, in Figure 10 (left), the eigenspectra normalized with the corresponding exact solutions are plotted for $g/L = 0.1 = \gamma$ for $p = 3, 4, 5, 6$ (with $n = 1, ..., N$ indexing

the eigenvalues). It can be clearly seen that the typical spectral convergence behavior of isogeometric Galerkin methods is realized in this problem as well. However, Figure 10 (right) presenting the normalized eigenspectra with $p = 3$ for different gradient parameter combinations of $g/L = 0, 0.01, 0.02$ and $\gamma/L = 0, 0.01, 0.02$ shows that the accuracy level is clearly parameter-dependent. It should be noticed that, as typical in isogeometric analysis, for B-spline basis functions with open knot vectors there exist high frequency outliers in Figure 10 (left) (with increasing magnitude and number along with the order of basis functions, as now visible for $p = 4, 5, 6$) constituting the discrete optical branch of the numerical spectrum. Outliers can be, however, eliminated by spacing control points uniformly (which requires a nonlinear reparametrization, however)[70].

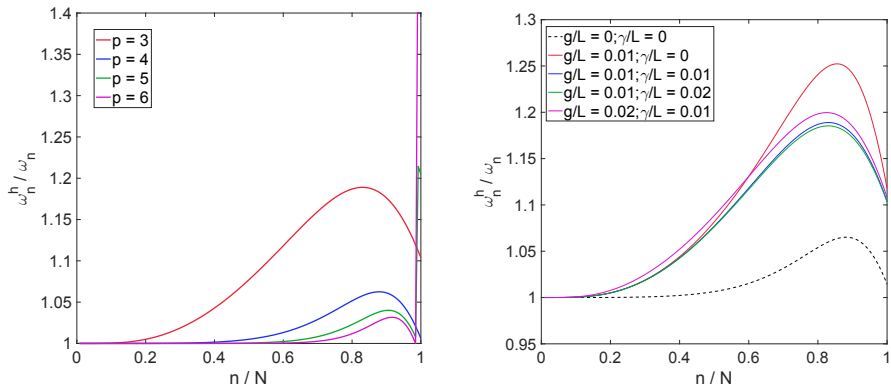

Figure 10. Doubly simply supported beam: (left) Discrete normalized spectra for $g/L = 0.1 = \gamma$ with $p = 3, 4, 5$ and 6; (right) Discrete normalized spectra with $p = 3$ for different gradient parameter combinations.

Size dependency of the effective Young's modulus for a cellular auxetic metamaterial

Let us consider a two-dimensional quadrangular strip under a uni-axial tensional loading: distributed vertical loadings act (in the y-direction) at the top and bottom boundary lines of the structure. Due to the symmetry of the loading and geometry, only one half of the model structure is analyzed, as depicted in Fig. 11 (left). The material of the structure is chosen to be an auxetic metamaterial architectured by using re-entrant (inverse) honeycomb cells composed of prismatic struts, having rectangular cross-sections with $A = t^2$, $I = t^4/12$ and $E = 110$ GPa (Titanium), for simplicity (see Fig. 11).

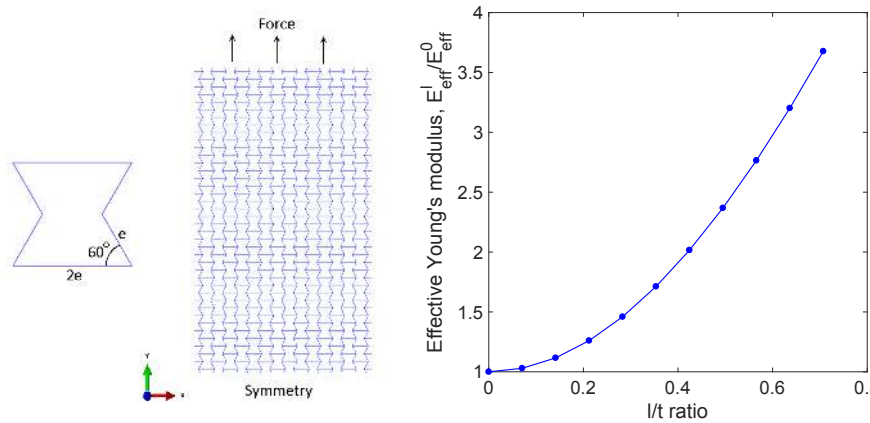

Figure 11. (left) Model structure composed of an auxetic metamaterial architectured by re-entrant honeycomb cells; (right) Size dependency of the relative effective Young's modulus.

First of all, it is well known that the mechanism of auxeticity in this type of cellular metamaterial originates from the topology of the re-entrant honeycomb cells exciting bending-dominated deformation states in the members forming the cell microstructure[8,9]. Accordingly, the strain energy of the uni-axially tensioned model structure is known to be dominated by the bending energy of the members: a numerical verification by standard finite element methods gives ratio $W_\mathrm{b}/W_\mathrm{s} = 33.1$, where W_b and W_s, respectively, denote the total bending and stretching energies of the members summed over the cell grid of the structure. The effective Poisson's ratio is known to be independent of the properties of the bulk material ($\nu = -\varepsilon_{xx}/\varepsilon_{yy} = -0.966$ for the present model structure), whereas in what follows we show how the effective Young's modulus of the strip depends on the scale of the members: with a fixed bulk material length scale l (see equation (71)), the strip becomes relatively stiffer when decreasing the thickness of the members and scaling the whole structure accordingly.

Since the model comparison in Section 5 shows that the stiffening of the second kind produces the thickness dependence of the bending rigidity, we model the structure by using members following the modified couple stress theory with the bending governing equation (66), or (67) with (71), in the form $EIc^l w^{(4)} = f$ with $EIc^l = EI(1 + 6l^2/t^2)$. The stiffening factor $c^l = 1 + 6l^2/t^2$ is given as a user-defined material value (connected to the moment of inertia) for a commercial finite element software (Comsol) using C^1-continuous Hermite elements for beam bending (cf. Section 5.1). Stretching of the members, decoupled from bending in case of linear elasticity, can be assumed to follow the classical elasticity theory giving the governing equation $EAu'' = Ab$ (with distributed axial loading b) since the sretching energy is negligible and since generalized bar models do not provide size-dependent stiffening effect of the second kind (see the derivation of the governing equation $EAu'' - g^2 EAu^{(4)} = Ab$ with analytical solutions and numerical methods in[56]).

Size dependency of the effective Young's modulus E_{eff}, defined as the ratio between the tensional loading and strain in the vertical direction, is presented in Fig. 11 (right) showing the cruciality of the stiffening effect for auxetic metamaterials obeying bending-dominated deformation.

7. Conclusions

In the theoretical part of the paper, displacement-based variational formulations and governing equations with boundary conditions are derived for a pair of Euler–Bernoulli beam bending models following a simplied form of Mindlin's strain gradient elasticity theory of form II. This leads to sixth-order boundary value problems with new types of boundary conditions which are given additional attributes *singly* and *doubly*; referring to a physically relevant distinguishment between free and prescribed curvature, respectively. By proving the continuity and ellipticity (coercivity) of the associated symmetric bilinear forms of the variational formulations, existence and uniqueness of weak solutions is established within an H^3 Sobolev space setting. For conforming Galerkin discretization methods, in particular, this is shown to guarantee invertible stiffness matrices and optimal convergence. Altogether, these theoretical results serve as a foundation for the development and analysis of numerical discretization methods as the one proposed in the second part of the paper.

In order to further disentangle the physicality of the models, the analyzed strain gradient formulations are next compared to other two generalized beam bending models which follow another modifed strain gradient elasticity theory and a modifed couple stress theory. First, it is explained how to extend the results of the variational analysis to cover these beam model variants. Second, the parameter dependence of the four models – with respect to the thickness and gradient parameters – is studied in detail by a model problem describing a cantilever beam. The comparison reveals essential features of these four closely related beam models: the reduced strain gradient formulation is essentially independent of the thickness parameter, whereas the other three models are able to present the thickness-dependent stiffening effect experimentally observed for micro- and nano-size cantilevers. Altogether, the comparison expresses that the ratio between the thickness and gradient parameters drastically affects the behavior of the models.

In the computational part of the paper, first the optimal convergence results of the theoretical part are confirmed by a conforming and isogeometric B-spline Galerkin discretization. In detail, for static problems the convergence rates in the H^3-norm follow the theoretical order $\mathcal{O}(h^{p-2})$ for a large range of gradient parameter values with C^{p-1}-continuous basis functions of order $p = 3, 4, 5$. Convergence in lower-order norms as well as convergence of eigenvectors and eigenvalues of free vibrations (for $p = 3, 4, 5, 6$) behave as expected as well. Parameter-dependent boundary layers, typical for solutions of problems following strain gradient elasticity theories, are addressed by numerical examples. Regarding free vibrations, the effect of gradient parameters and the role of rotatory inertia terms are shown to be significant for obtaining physically meaningful dispersion curves, in particular.

Finally, we demonstrate the cruciality of the stiffening effect for auxetic metamaterials obeying bending-dominated deformation of cell struts: the effective Young's modulus is shown to be prominently size-dependent in the presence of micro- and nano-beams as cell members. The numerical results – together with the model comparison – call for further experimental model validations with respect to both different engineering materials and various micro-structural length scales. Altogether, the modern numerical methods proposed here provide reliable and efficient general-purpose tools for solving complex problems which are difficult to solve by analytical means dominating the literature related to the topic.

Acknowledgements

The first, the second and the fourth author have been supported by Academy of Finland through a project entitled Adaptive isogeometric methods for thin-walled structures (decisions 270007, 273609, 304122).

References

1. Yurish SY. *Sensors and Biosensors, MEMS Technologies and its Applications, Book Series: Advances in Sensors: Reviews, Vol. 2*. International Frequency Sensor Association Publishing, 2013.
2. Bogue R. Recent developments in MEMS sensors: a review of applications, markets and technologies. *Sensor Review* 2013; 33: 300–304.
3. Bogue R. Towards the trillion sensors market. *Sensor Review* 2014; 34: 137–142.
4. Espinosa HD, Bernal RA and Minary-Jolandan M. A review of mechanical and electromechanical properties of piezoelectric nanowires. *Advanced Materials* 2012; 24: 4656–4675.
5. Harris KD, Elias AL and Chung HJ. Flexible electronics under strain: a review of mechanical characterization and durability enhancement strategies. *Journal of Material Science* 2016; 55: 2771–2805.
6. Tian W, Zhang X, Chen Z et al. A review of graphene on NEMS. *Recent Patents on Nanotechnology* 2016; 10: 3–10.
7. O'Donnell J, Kim M and Yoon HS. A review on electromechanical devices fabricated by additive manufacturing. *Journal of Manufacturing Science and Engineering* 2017; 139: 010801–3.
8. Prawoto Y. Seeing auxetic materials from the mechanics point of view: A structural review on the negative Poisson's ratio. *Computational Materials Science* 2012; 58: 140–153.
9. Desmoulins A, Zelhofer A and Kochmann DM. Auxeticity in truss networks and the role of bending versus stretching deformation. *Smart Materials and Structures* 2016; 25: 054003.
10. Rafiee R and Moghadam RM. On the modeling of carbon nanotubes: A critical review. *Composites: Part B* 2014; 56: 435–449.
11. Arash B and Wang Q. A review on the application of nonlocal elastic models in modeling of carbon nanotubes and graphenes. *Computational Materials Science* 2012; 51: 303–313.

12. Wang KF, Wang BL and Kitamura T. A review on the application of modified continuum models in modeling and simulation of nanostructures. *Acta Mechanica Sinica* 2016; 32: 83–100.
13. Young RJ, Kinloch IA, Gong L et al. The mechanics of graphene nanocomposites: A review. *Composites Science and Technology* 2012; 72: 1459–1476.
14. Sakhaee-Pour A, Ahmadian MT and AVafai. Vibrational analysis of single-walled carbon nanotubes using beam element. *Thin-Walled Structures* 2009; 47: 646–652.
15. Lee J and Lee B. Modal analysis of carbon nanotubes and nanocones using FEM. *Computational Materials Science* 2012; 51: 30–42.
16. Maugin GA. Generalized continuum mechanics: What do we mean by that? In Maugin GA and Metrikine AV (eds.) *Mechanics of Generalized Continua, One Hundred Years After the Cosserats*. Springer, 2010. pp. 3–14.
17. Maugin GA. A historical perspective of generalized continuum mechanics. In Altenbach H, Maugin GA and Erofeev V (eds.) *Mechanics of Generalized Continua*. Springer, pp. 3–14.
18. Niiranen J and Niemi AH. Variational formulation and general boundary conditions for sixth-order boundary value problems of gradient-elastic Kirchhoff plates. *European Journal of Mechanics A/Solids* 2017; 61: 164–179.
19. Khakalo S and Niiranen J. Gradient-elastic stress analysis near cylindrical holes in a plane under bi-axial tension fields. *International Journal of Solids and Structures* 2017; 110-111: 351–366.
20. Fernández-Sáez J, Zaera R, Loya J et al. Bending of Euler–Bernoulli beams using Eringens integral formulation: A paradox resolved. *International Journal of Engineering Science* 2016; 99: 107–116.
21. Askes H and Aifantis EC. Gradient elasticity in statics and dynamics: An overview of formulations, length scale identification procedures, finite element implementations and new results. *International Journal of Solids and Structures* 2011; 48: 1962–1990.
22. Papargyri-Beskou S, Polyzos D and Beskos DE. Wave dispersion in gradient elastic solids and structures: A unified treatment. *International Journal of Solids and Structures* 2009; 40: 385–400.
23. Eltaher MA, Khater ME and Emam SA. A review on nonlocal elastic models for bending, buckling, vibrations, and wave propagation of nanoscale beams. *Applied Mathematical Modelling* 2016; 40: 4109–4128.
24. Lam DCC, Yang F, Chong ACM et al. Experiments and theory in strain gradient elasticity. *Journal of the Mechanics and Physics of Solids* 2003; 51: 1477–1508.
25. McFarland AW and Colton JS. Role of material microstructure in plate stiffness with relevance to microcantilever sensors. *Journal of Micromechanics and Microengineering* 2005; 15: 1060–1067.
26. Liebold C and Müller WH. Applications of strain gradient theories to the size effect in submicro-structures incl. experimental analysis of alastic material parameters. *Bulletin of TICMI* 2015; 19: 45–55.
27. Jing GY, Duan HL, Sun XM et al. Surface effects on elastic properties of silver nanowires: Contact atomic-force microscopy. *Physical Review B* 2006; 73: 235409.
28. Chen CQ, Shi Y, Zhang YS et al. Size dependence of Young's modulus in zno nanowires. *Physical Review Letters* 2006; 96: 1–4.

29. Aifantis EC. Exploring the applicability of gradient elasticity to certain micro/nano reliability problem. *Microsystem Technologies* 2009; 15: 109–115.
30. Papargyri-Beskou S, Tsepoura KG, Polyzos D et al. Bending and stability analysis of gradient elastic beams. *International Journal of Solids and Structures* 2003; 46: 3751–3759.
31. Vardoulakis I, Exadaktylos G and Aifantis E. Gradient elasticity with surface energy: mode-iii crack problem. *International Journal of Solids and Structures* 1996; 30: 4531–4559.
32. Altan BS and Aifantis EC. On some aspects in the special theory of gradient elasticity. *Journal of the Mechanical Behavior of Materials* 1997; 8: 231–282.
33. Vardoulakis I and Sulem J. *Bifurcation Analysis in Geomechanics*. London: Blackie/Chapman and Hall, 1995.
34. Park SK and Gao XL. Bernoulli–Euler beam model based on a modified couple stress theory. *Journal of Micromechanics and Microengineering* 2006; 16: 2355–2359.
35. Yang F, Chong A, Lam D et al. Couple stress based strain gradient theory for elasticity. *International Journal of Solids and Structures* 2002; 39: 2731–2743.
36. Gao XL and Mahmoud FF. A new Bernoulli–Euler beam model incorporating microstructure and surface energy effects. *Zeitschrift für angewandte Mathematik und Physik* 2014; 65: 393–404.
37. Gurtin ME and Murdoch AI. Surface stress in solids. *International Journal of Solids and Structures* 1978; 14: 431–440.
38. Kong S, Zhou S, Nie Z et al. Static and dynamic analysis of micro beams based on strain gradient elasticity theory. *International Journal of Engineering Science* 2009; 47: 487–498.
39. Akgöz B and Civalek Ö. Analysis of micro-sized beams for various boundary conditions based on the strain gradient elasticity theory. *Archive of Applied Mechanics* 2012; 82: 423–443.
40. Lazopoulos KA and Lazopoulos AK. Bending and buckling of thin strain gradient elastic beams. *European Journal of Mechanics A/Solids* 2010; 29: 837–843.
41. Liang X, Hu S and Shen S. A new Bernoulli–Euler beam model based on a simplified strain gradient elasticity theory and its applications. *Composite Structures* 2014; 111: 317–323.
42. Gao XL and Park S. Variational formulation of a simplified strain gradient elasticity theory and its application to a pressurized thick-walled cylinder problem. *International Journal of Solids and Structures* 2007; 44: 7486–7499.
43. Ma HM, Gao XL and Reddy JN. A microstructure-dependent Timoshenko beam model based on a modified couple stress theory. *Journal of the Mechanics and Physics of Solids* 2008; 56: 3379–3391.
44. Yaghoubi ST, Mousavi S and Paavola J. Strain and velocity gradient theory for higher-order shear deformable beams. *Archive of Applied Mechanics* 2015; 85: 877–892.
45. Yaghoubi ST, Mousavi S and Paavola J. Size effects on centrosymmetric anisotropic shear deformable beam structures. *ZAMM Journal of Applied Mathematics and Mechanics* 2017; 97: 586601.
46. Yaghoubi ST, Balobanov V, Mousavi S et al. Variational formulations and isogeometric analysis for the dynamics of anisotropic gradient-elastic Euler–Bernoulli and shear-deformable beams. *to appear in European Journal of Mechanics A/Solids* 2017; .
47. Alibert J, Seppecher P and dell'Isola F. Truss modular beams with deformation energy depending on higher displacement gradients. *Mathematics and Mechanics of Solids* 2003; 8: 51–73.

48. Seppecher P, Alibert JJ and dell'Isola F. Linear elastic trusses leading to continua with exotic mechanical interactions. *Journal of Physics: Conference Series* 2011; 319.
49. Carcaterra A, dell'Isola F, Esposito R et al. Macroscopic description of microscopically strongly inhomogenous systems: A mathematical basis for the synthesis of higher gradients metamaterials. *Archive for Rational Mechanics and Analysis* 2015; 218: 1239–1262.
50. Giorgio I, Corte AD and dell'Isola F. Dynamics of 1D nonlinear pantographic continua. *Nonlinear Dynamics* 2017; 88: 21–31.
51. Mindlin RD. Micro-structure in linear elasticity. *Archive for Rational Mechanics and Analysis* 1964; 16: 51–78.
52. Mir M, Papargyri-Beskou S and Beskos DE. Finite element static and stability analysis of gradient elastic beam structures. *Acta Mechanica* 2015; 226: 745–768.
53. Thai HT, Vo TP, Nguyen TK et al. A review of continuum mechanics models for size-dependent analysis of beams and plates. *Composite Structures* 2017; 177: 196–219.
54. Eringen AC. On differential equations of nonlocal elasticity and solutions of screw dislocation and surface waves. *Journal of Applied Physics* 1983; 54: 4703–4710.
55. Tuna M and Kirca M. Exact solution of Eringens nonlocal integral model for bending of Euler–Bernoulli and Timoshenko beams. *International Journal of Engineering Science* 2016; 105: 80–92.
56. Niiranen J, Khakalo S, Balobanov V et al. Variational formulation and isogeometric analysis for fourth-order boundary value problems of gradient-elastic bar and plane strain/stress problems. *Computer Methods in Applied Mechanics and Engineering* 2016; 308: 182–211.
57. Kiendl J, Auricchio F, Hughes T et al. Single-variable formulations and isogeometric discretizations for shear deformable beams. *Comp Meths Appl Mech Engrg* 2015; 284: 988–1004.
58. Niiranen J, Kiendl J, Niemi AH et al. Isogeometric analysis for sixth-order boundary value problems of gradient-elastic Kirchhoff plates. *Computer Methods in Applied Mechanics and Engineering* 2017; 316: 328–348.
59. Greco L and Cuomo M. B-spline interpolation of Kirchhoff–Love space rods. *Computer Methods in Applied Mechanics and Engineering* 2013; 256: 251–269.
60. Beirão da Veiga L, Hughes T, Kiendl J et al. A locking-free model for Reissner–Mindlin plates: Analysis and isogeometric implementation via NURBS and triangular NURPS. *Math Meth Appl Sci* 2015; 25: 1519–1551.
61. Khakalo S and Niiranen J. Isogeometric analysis of higher-order gradient elasticity by user elements of a commercial finite element software. *Computer-Aided Design* 2017; 82: 154–169.
62. Beheshti A. Large deformation analysis of strain-gradient elastic beams. *Computers and Structures* 2016; 177: 162–175.
63. Lazar M and Maugin GA. Nonsingular stress and strain fields of dislocations and disclinations in first strain gradient elasticity. *International Journal of Engineering Science* 2005; 43: 1157–1184.
64. Mindlin RD. Second gradient of strain and surface-tension in linear elasticity. *International Journal of Solids and Structures* 1965; 1: 417–438.
65. Bleustein JL. A note on the boundary conditions of Toupin's strain-gradient theory. *International Journal of Solids and Structures* 1967; 3: 1053–1057.

66. Dehrouyeh-Semnani AM and Nikkhah-Bahrami M. A discussion on incorporating the Poisson effect in microbeam models based on modified couple stress theory. *International Journal of Engineering Science* 2015; 86: 20–25.
67. Polizzotto C. A gradient elasticity theory for second-grade materials and higher order inertia. *International Journal of Solids and Structures* 2012; 49: 2121–2137.
68. Braess D. *Finite Elements. Theory, fast solvers, and applications in solid mechanics*. Cambridge: Cambridge University Press, 2001.
69. Hughes TJR, Cottrell JA and Bazilevs Y. Isogeometric analysis: Cad, finite elements, nurbs, exact geometry and mesh refinement. *Comput Methods Appl Mech Engrg* 2005; 194: 4135–4195.
70. Cottrell JA, Reali A, Bazilevs Y et al. Isogeometric analysis of structural vibrations. *Computer Methods in Applied Mechanics and Engineering* 2006; 195: 5257–5296.

Normalized bending rigidities for model comparison

The normalized bending rigidities plotted in Figure 1 have the following forms: for the full SG-model, it holds that

$$(D/D_0)^{-1} = \frac{g^2}{L^2}\,\frac{\alpha(L^2/t^2)-3+(L^2/g^2)}{(\alpha g^2/t^2+1)^2} + \frac{3g^3}{2L^3}\,\frac{\alpha(L^2/t^2)(g^2/t^2+1)+4}{(\alpha g^2/t^2+1)^{5/2}}\,\frac{\cosh\sqrt{\alpha(L^2/t^2+L^2/g^2)}-1}{\sinh\sqrt{\alpha(L^2/t^2+L^2/g^2)}}; \tag{79}$$

for the reduced SG-model, it holds that

$$D/D_0 = \frac{\sinh(L/g)}{\sinh(L/g)(1-3g^2/L^2)+6(g^3/L^3)(\cosh(L/g)-1)}; \tag{80}$$

for the modified SG-model, it holds that

$$(D/D_0)^{-1} = \frac{1+c\alpha l^2/t^2-3dl/L^2}{1+c\alpha l^2/t^2} + \frac{6l^3}{L^3}\,\frac{d^{3/2}}{(1+c\alpha l^2/t^2)^{5/2}}\,\frac{\cosh\sqrt{(L^2/d)(1/l^2+c\alpha/t^2)}-1}{\sinh\sqrt{(L^2/d)(1/l^2+c\alpha/t^2)}}; \tag{81}$$

for the modified CS-model, the normalized bending rigidity takes the simplest form

$$D/D_0 = 1+\frac{\alpha l^2}{2t^3}. \tag{82}$$